# Synchronization of Belousov–Zhabotinsky oscillators with electrochemical coupling in a spontaneous process

Cite as: Chaos 32, 093128 (2022); https://doi.org/10.1063/5.0096689 Submitted: 20 April 2022 • Accepted: 22 August 2022 • Published Online: 20 September 2022

Yifan Liu, Juan Pérez-Mercader and 🔟 István Z. Kiss

### COLLECTIONS

Paper published as part of the special topic on From Chemical Oscillations to Applications of Nonlinear Dynamics: Dedicated to Richard J. Field on the Occasion of his 80th Birthday







ARTICLES YOU MAY BE INTERESTED IN

Detecting bifurcations in dynamical systems with CROCKER plots Chaos: An Interdisciplinary Journal of Nonlinear Science 32, 093111 (2022); https:// doi.org/10.1063/5.0102421

Transport and nonequilibrium phase transitions in polygonal urn models Chaos: An Interdisciplinary Journal of Nonlinear Science 32, 093127 (2022); https:// doi.org/10.1063/5.0101933

Application of the Slater criteria to localize invariant tori in Hamiltonian mappings Chaos: An Interdisciplinary Journal of Nonlinear Science 32, 093125 (2022); https:// doi.org/10.1063/5.0103427





# Synchronization of Belousov-Zhabotinsky oscillators with electrochemical coupling in a spontaneous process

Cite as: Chaos 32, 093128 (2022); doi: 10.1063/5.0096689 Submitted: 20 April 2022 · Accepted: 22 August 2022 · Published Online: 20 September 2022







Yifan Liu, Juan Pérez-Mercader, 1,2 and István Z. Kiss<sup>3,a)</sup> 📵

#### **AFFILIATIONS**

- Department of Earth and Planetary Sciences, Harvard Origins of Life Initiative, Harvard University, 20 Oxford Street, Cambridge, Massachusetts 02138, USA
- <sup>2</sup>Santa Fe Institute, Santa Fe, New Mexico 87501, USA
- Department of Chemistry, Saint Louis University, 3501 Laclede Ave., St. Louis, Missouri 63103, USA

Note: This article is part of the Focus Issue, From Chemical Oscillations to Applications of Nonlinear Dynamics: Dedicated to Richard J. Field on the Occasion of his 80th Birthday.

a) Author to whom correspondence should be addressed: istvan.kiss@slu.edu

# **ABSTRACT**

A passive electrochemical coupling approach is proposed to induce spontaneous synchronization between chemical oscillators. The coupling exploits the potential difference between a catalyst redox couple in the Belousov-Zhabotinsky (BZ) reaction, without external feedback, to induce surface reactions that impact the kinetics of the bulk system. The effect of coupling in BZ oscillators under batch condition is characterized using phase synchronization measures. Although the frequency of the oscillators decreases nonlinearly over time, by a factor of 2 or more within 100 cycles, the coupling is strong enough to maintain synchronization. In such a highly drifting system, the Gibbs-Shannon entropy of the cyclic phase difference distribution can be used to quantify the coupling effect. We extend the Oregonator BZ model to account for the drifting natural frequencies in batch condition and for electrochemical coupling, and numerical simulations of the effect of acid concentration on synchronization patterns are in agreement with the experiments. Because of the passive nature of coupling, the proposed coupling scheme can open avenues for designing pattern recognition and neuromorphic computation systems using chemical reactions in a spontaneous process.

Published under an exclusive license by AIP Publishing. https://doi.org/10.1063/5.0096689

Oscillations of concentration of chemical species often occur in chemical reactions with autocatalysis at far from thermodynamic equilibrium. In two systems in the presence of coupling, synchronization can take place when the period of oscillations settles to a common value. In many previous studies, to facilitate synchronization studies, the system was held in this far-from-equilibrium state in an open system (so that the oscillations are maintained for long periods) and/or coupling was intensified with external feedback or pumps. Here, we show that a redox oscillatory chemical reaction in two beakers can spontaneously synchronize with a connecting metal wire in a closed system. The coupling takes place by mediating electrochemical reactions on the two ends of the metal wire. The results demonstrate the use of synchronization theories in a highly drifting system (as the equilibrium is reached) and set the stage for the design of large sets of coupled chemical

reactions, e.g., for chemical computations, without complicated experimental designs.

### I. INTRODUCTION

Coupled complex chemical reactions demonstrate a vast range of nonlinear phenomena, including Turing patterns, waves, clusters, and chaos.<sup>1,2</sup> Two different types of coupling means are generally used: one is the chemical approach through a shared reactant that links two reactions occurring in the same reactor and the other is to use physical coupling that includes mass transfer, electrical coupling, or external constraints in separate reactors.3 Coupled systems have been the subject of extensive studies both in theory and in experiment as they exhibit complex forms of patterns in the

whole range between incoherence and complete synchronization. On one hand, chemical reaction-diffusion systems represent local coupling through concentration gradients, where the change of concentration affects only the local dynamics of the system. On the other hand, global coupling forms when a change in part of the system can be felt equally by all other parts. This can usually be obtained in chemical reactions through controlled temperature or by long-range electrical coupling in electrochemical systems. (5.7)

The Belousov-Zhabotinsky (BZ) reaction is an extensively studied and relatively well-understood chemical oscillator.<sup>8-10</sup> Based on the knowledge of the single oscillator, coupled oscillators have been investigated through various coupling methods. Active chemical coupling of BZ oscillators was utilized in continuous stirred tank reactors (CSTR), where the mass exchange rate between the cells can be controlled by the active feed rate. 11,12 In such a system, in-phase and out-of-phase synchronization as well as oscillator death were found by varying the coupling strength.<sup>13</sup> However, the coupling can also be passive and depends only on mass transfer without continuous feeding of reactants. For example, a similar experimental setup was used in batch conditions to observe phase-locking behavior of coupled BZ reactions.14 The BZ reaction, in particular, with beads and droplets, served an important vehicle for studying synchronization patterns, for example, Kuramoto and dynamical quorum sensing transitions, clustering, and chimera (co-existing synchronized and desynchronized oscillatory) states.<sup>2,15–20</sup>

Similarly, studies involving active and passive coupling were also carried out in electrochemical reactions with electrode arrays.21-30 Active coupling was implemented by potential or current feedback through a potentiostat. A delay-coupled network of oscillators exhibited amplitude death, and upon removal of the feedback, the oscillations were restored to maintain antiphase synchronization.<sup>31</sup> Passive coupling in electrochemistry utilizes capacitance or resistance to achieve synchronization.<sup>32–3</sup> addition to Kuramoto and quorum sensing transitions, phase and frequency clusters and several different forms of chimeras were identified. 7,32,37-41 It was also shown in previous research that the intrinsic resistance of migration currents in microfluidic channels can play the role of collective resistance, and the coupling strength can, thus, be changed by tuning the position of electrodes. 42 Through different placements of the electrodes, localized current oscillation can be observed.43

Alternatively, it is also possible to couple chemical oscillators through an electrochemical methods. 44 This provides an alternative path to explore various coupling effects and novel pattern formations. The basic concept of electrochemically coupled BZ reactions has been proposed by Crowley and Field, who carried out simulations and presented some interesting phenomena including chaotic oscillation. 44 The concept was demonstrated experimentally later through active feedback in BZ oscillators. 45,46 The active electrical coupling was implemented using a galvanostat that monitors the electrode potential of the BZ system and injects current to the reactors based on a feedback rule. 47,48 Such device can open avenues for the design of pattern recognition. 49-53 However, for practical applications, for example, consisting of a large-scale system with thousands of chemical oscillators for sensing and information processing, it would be highly desirable to design sufficiently strong coupling that

can impact oscillator dynamics without external monitoring and feedback circuitry.

In this paper, we explore the effect of electrochemical coupling on chemical oscillators without an active feedback, i.e., in a spontaneous process driven by electrochemical potential gradients. Two BZ oscillators are coupled through Pt meshes in an H-cell separated by a frit. Their coupling was driven by the redoxpotential difference between the oxidation states of the metal catalyst  $[Ru(bpy)_3^{2+}/Ru(bpy)_3^{3+}]$ . Due to this potential difference, a current flows between the two compartments of the cell, which is proportional to their instantaneous difference in redox potential. This provides a convenient way of coupling two chemical oscillators, in which potentiostats/galvanostats are not necessary. The phase and amplitude dynamics of two BZ oscillators under batch condition are first determined without passive coupling. Then, the effect of coupling is characterized using phase synchronization measures. Finally, a modified Oregonator model with five variables and passive electrical coupling is developed to account for synchronization patterns.

#### II. MATERIAL AND METHODS

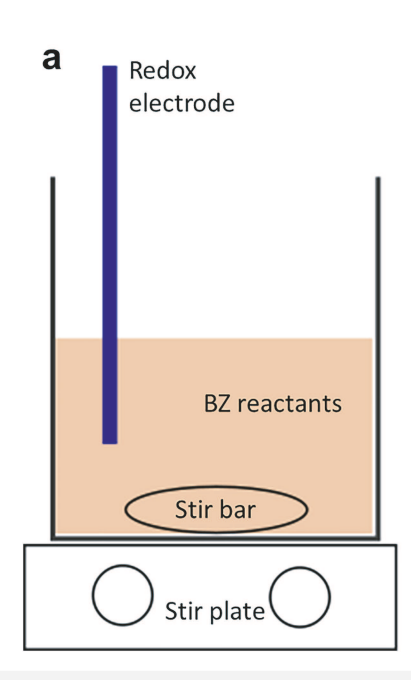
#### A. Reactors

All experiments were performed at room temperature (18 °C-22 °C), and the experimental setup is shown in Fig. 1. Figure 1(a) shows a single BZ reaction in the beaker. A stir bar was placed at the center of the beaker with a stirring rate of 500 rpm. A monitoring redox electrode (Microelectrodes, Inc.) was placed close to the stir bar on the side of the beaker. The redox electrode consists of a Pt working electrode and a Ag/AgCl/3M KCl reference electrode. Experiments with two BZ oscillators were performed in the H-cell (Pine Research Instrumentation) as shown in Fig. 1(b). The cell consists of two cylindrical compartments separated by a fritted disk. On each side of the cell, a stir bar was placed rotating clockwise with a rate of 500 rpm. A  $4 \times 9$  cm Pt mesh was rolled and fit around the inner diameter of each compartment for coupling, and the circuit was completed by a metal connecting wire between the meshes. For electrochemically isolated reactions, the Pt meshes were sill present in the cell while the connection was open. The reaction on the left side of the H-cell is denoted as "oscillator 1."

# **B.** Materials

The chemicals used in experiments with low acid concentration were 3 ml 5M  $\rm H_2SO_4$  (10N/5M, Fisher Chemical), 0.4 ml 12.5 mM  $\rm Ru(byp)_3Cl_2(_6H_2O)$  (Sigma Aldrich), 1 ml 2 M NaBrO<sub>3</sub> (Alfa Aesar), and 0.5 ml 3.5 M  $\rm CH_2(COOH)_2$  (Sigma Aldrich) in 16.6 ml water. With high acid concentration, there were 6 ml 5 M  $\rm H_2SO_4$  and 13.6 ml water, and all other species remained at same concentrations.

Experiments in the beaker were prepared by mixing  $H_2SO_4$  in water first and then adding  $Ru(byp)_3Cl_2(_6H_2O)$ ,  $NaBrO_3$ , and  $CH_2(COOH)_2$  sequentially. The total volume in the beaker is 21.5 ml. For experiments in the H-cell, all the volumes were doubled and the reactants were pre-mixed in the same sequence in a stirred beaker. After 10 min, the pre-mixed solution was dispensed evenly



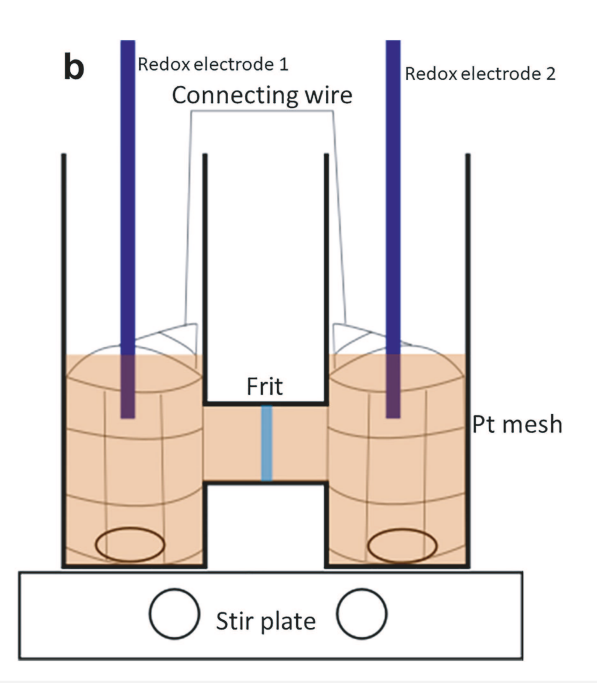


**FIG. 1.** Experimental setup. (a) Schematic diagram of a single BZ oscillator in a beaker. The redox electrode consists of a Pt working electrode and a Ag/AgCl 3 M KCl reference electrode. (b) Schematic diagram of two BZ oscillators in the H-cell. Each compartment of the H-cell has a redox electrode similar to the one in (a). A Pt mesh  $(4 \times 9 \text{ cm})$  is rolled and fit into the inner diameter of the compartment on each side. The two Pt meshes are connected through a metal wire for electrochemically coupled experiments. For electrochemically isolated experiments, the connection between the two meshes is open.

to the two compartments of the H-cell, making the volume in each compartment 21.5 ml.

# C. Selection of observables and interpretation of data

The redox electrodes were connected to a data acquisition board (National Instruments USB-6343), and the output of the redox potential was monitored and recorded through a Labview interface on a computer. The oscillations of the redox potential were characterized by amplitude, frequency, and phase, which were all calculated based on the position (in time) and height (in redox potential) of peaks. If  $t_n$  and  $t_{n+1}$  are the timings of nth and (n+1)th peaks, and every two successive peaks are separated by  $2\pi$ , then the phase  $(\phi)$  is defined as

$$\phi(t) = \frac{t - t_n}{t_{n+1} - t_n} 2\pi (2n - 1), \quad t_n < t < t_{n+1}, \quad n = 1, 2, 3, \dots$$
(1)

Amplitude is defined as the peak to trough distance; frequency is calculated by taking the mean value of the inverse period of each cycle, where the period is the difference in the timing of each successive peak.

For coupled oscillators, phase difference  $(\Delta \phi)$ , probability distribution  $(p_k)$  of the remainder of phase difference  $(\Delta \phi_{mod})$ , and entropy (S) were used to characterize the coupling effect. Phase difference  $\Delta \phi = \phi_1 - \phi_2$ , where  $\phi_1$  and  $\phi_2$  are the phases of oscillators 1 and 2.  $\Delta \phi_{mod}$  is the remainder of  $\Delta \phi$  divided by  $2\pi$ .  $p_k = n_k/N$  is the probability of  $\Delta \phi_{mod}$ , where  $n_k$  is the number of counts in bin

k ( $k=1,2,3,\ldots,36$ ); N is the total number of counts; all bins are equally spaced with a width of  $\frac{2\pi}{36}$ . The Gibbs–Shannon entropy is then given by

$$S = -\sum_{k=1}^{36} p_k \ln p_k, \tag{2}$$

with a maximum value  $S_{max} = -\ln \frac{1}{k} = 3.58$ .

Note that other measures of synchronization could also be applied, in particular, the widely used Kuramoto order parameter, which is an excellent choice for oscillator populations. We have opted for the Gibbs–Shannon entropy of the phase difference because it was shown to be effective for a pair of coupled oscillators for complex (even chaotic) dynamics.<sup>35</sup>

# III. RESULTS AND DISCUSSION

# A. Experiments

### 1. Single BZ oscillator

We start with a single BZ oscillatory reaction under batch condition, and the evolution of redox potential vs time is shown in Fig. 2(a). The peak redox potential in the complete time series remains relatively constant at 1.1 V, while the trough gradually increases from 0.86 to 0.94 V. This causes a 29% decrease in amplitude as shown in Fig. 2(c) from 0.24 to 0.17 V. The period of oscillations, on the other hand, increases during 108 cycles as shown

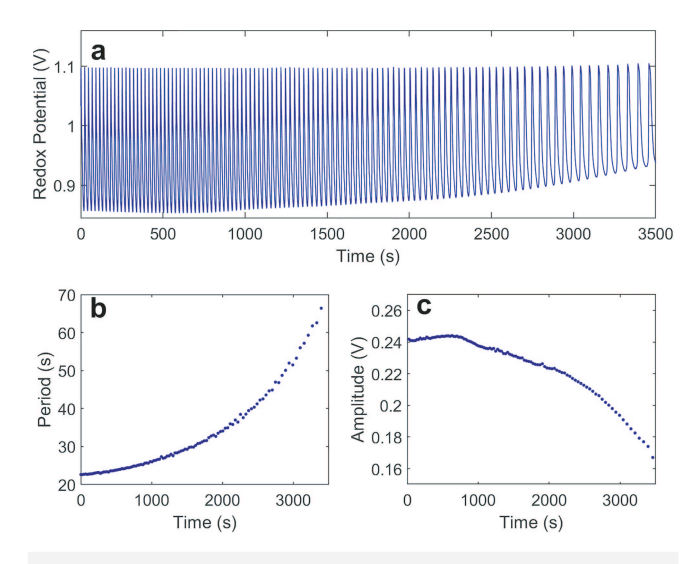


**FIG. 2.** Single BZ oscillator in the beaker with low acid concentration ([ $H_2SO_4$ ] = 0.7M). (a) Evolution of redox potential vs time. (b) Instantaneous period vs time. (c) Instantaneous amplitude vs time. The concentrations of other species remain the same in all experiments: [Ru(bpy) $_3Cl_2$ ] = 0.23 mM, [NaBrO $_3$ ] = 93 mM, [CH $_2$ (COOH) $_2$ ] = 81 mM.

in Fig. 2(b). At the beginning, the period is about 23 s and it gradually increases by 22% to 28 s at the 54th cycle (1301 s). After that, the period shows a 187% increase and reaches 66 s at the end of the time series. The average period over the whole time series is 30 s (0.0338 Hz). We then examine the coupling effect of two oscillators in such a highly drifting system.

# 2. Effect of coupling with low acid concentration

Figure 3(a) shows the oscillations of two electrochemically isolated BZ reactions in the H-cell. Due to different sensitivities of redox electrodes, the redox potentials of the two oscillatory reactions show slightly different amplitudes. The phase difference between the two oscillators is shown in Fig. 3(b). A non-monotonic variation with a minimum value is observed: The phase difference decreases at the beginning and starts to increase at around 1500 s. This is due to the frequency drift under batch condition described in Fig. 2. With uncoupled oscillators with linear, identical drifting in their frequencies, it would be expected that one of the oscillators is faster than the other, in spite of the change in their natural frequencies over time. This would result in a monotonic change in the phase difference. However, in the experiments, we observed that, when the reaction starts, one oscillator shows higher natural frequency and the other one is lower. During the reaction, both oscillators slow down but at a different rate (i.e., the frequency of the faster oscillator decreases at a higher rate than the slower one). This causes the faster oscillator to be slower toward the end while the slower one becomes relatively faster. The frequencies of the oscillators gradually approach each other and intersect at the trough on the curve.

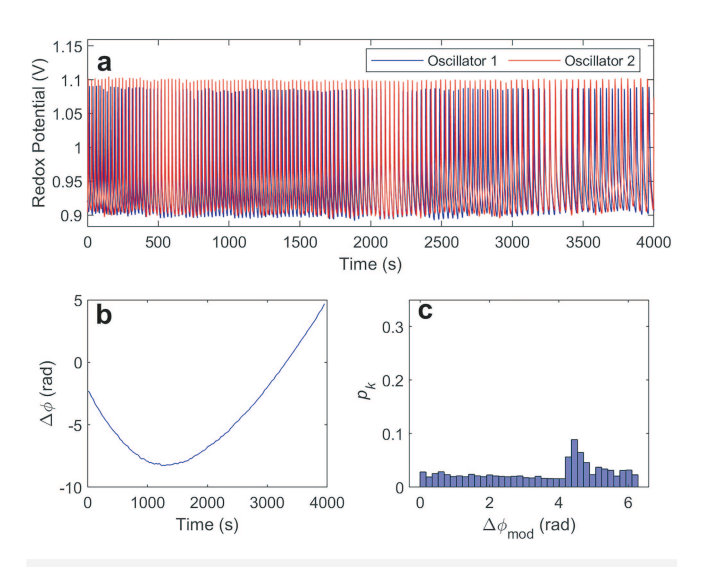


**FIG. 3.** Two electrochemically isolated BZ oscillators in the H-cell with low acid concentration ([H<sub>2</sub>SO<sub>4</sub>] = 0.7M). (a) Evolution of redox potential vs time. (b) Phase difference vs time. (c) Probability distribution of  $\Delta\phi_{mod}$  (the remainder of phase difference divided by  $2\pi$ ).

The probability distribution  $(p_k)$  of phase difference (over the range of 0– $2\pi$  rad) for uncoupled oscillators should be flat. However, owing to the drifting effect,  $p_k$  shows a small peak (0.09) around 4.5 rad in Fig. 3(c). The entropy is 3.47, calculated by Eq. (2), which is 97% of  $S_{max}$  (3.58).

We repeated the experiment twice under the same conditions and found different peak positions as shown in Fig. 4. In Figs. 4(a) and 4(b), there is a small peak close to 0.1 (0.11 and 0.09). While the entropy in both cases is close to 3.45 [Fig. 4(a)] and 3.46 [Fig. 4(b)], the positions of the peaks are different at 3.4 and 5.3 rad, respectively. The position of the peaks is dependent on the initial conditions; it is, thus, likely that the peaks represent a phase difference at which the two slowly drifting oscillators happen to have the same frequency. Thus, in this case, the small peak observed in the phase difference histogram is not related to a synchronization behavior but can be interpreted as a result of the uneven drift of the intrinsic frequency of the uncoupled oscillators.

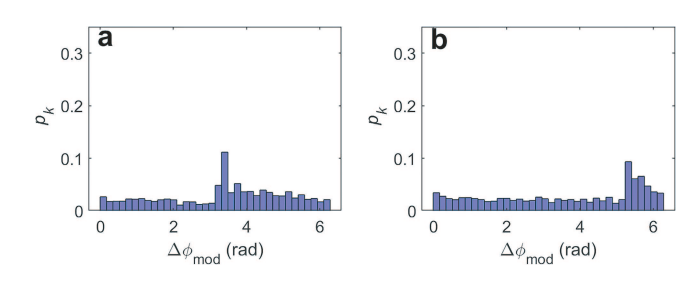


**FIG. 4.** Repeated experiments without coupling with low acid concentration ([ $H_2SO_4$ ] = 0.7M). (a) Probability distribution of  $\Delta\phi_{mod}$  with a peak at around  $\pi$ . (b) Experiment with a peak at round  $2\pi$ .

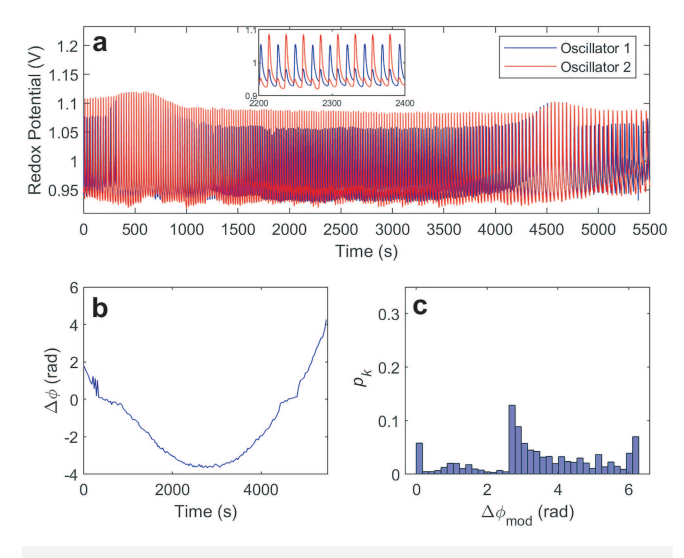


**FIG. 5.** Two electrochemically coupled BZ oscillators in the H-cell with low acid concentration ([ $H_2SO_4$ ] = 0.7 M). (a) Evolution of redox potential vs time. Inset panel shows a zoomed-in time series of redox potential from 2200 to 2400 s. (b) Phase difference vs time. (c) Probability distribution of  $\Delta\phi_{mod}$ .

When the two oscillators are coupled electrochemically, as shown in Fig. 5, some effects were observed while there is no full synchronization (i.e., phase locking for the entire experiment). The amplitudes of both oscillators increase when their phases coincide on top of each other at around 580 and 4580 s. Additionally, as shown on the inset panel in Fig. 5(a), each oscillator has small peaks driven by the other oscillator besides natural oscillations. In the middle region of the time series (from 2000 to 3500 s), the oscillators show anti-phase synchronization for 1500 s before the phases start to drift. The phase changes are also reflected in Fig. 5(b). Two plateaus where  $\Delta \phi = 0$  are located at around 580 and 4580 s. In the middle region from 2000 to 3500 s, the phase difference is relatively flat around  $-\pi$ , which indicates the anti-phase position of the peaks. The probability distribution of  $\Delta \phi_{mod}$  in Fig. 5(c) shows a slightly higher peak of 0.13 at 2.7 rad compared to 0.09 in Fig. 3(c). The entropy, thus, shows a slight decrease to 3.22, which is 89.9% of  $S_{max}$ . Although a peak is seen in the figure,  $\Delta \phi_{mod}$  still expands over the entire region of  $0-2\pi$  rad, which indicates that there is little, but measurable synchronization effect.

# 3. Effect of coupling with high acid concentration

The experimental results with low acid concentrations implied that in order to synchronize the two oscillators in such a highly drifting system, a stronger coupling strength is required. One way to explore the coupling strength in an acidic environment is to increase the concentration of acid. We doubled the concentration of  $H_2SO_4$ , and the evolution of redox potential is shown in Fig. 6(a) without coupling. As the concentration of acid increases, the amplitude of oscillations becomes more irregular. Although the phase difference shown in Fig. 6(b) has more noise than similar figures in low concentration, the drift in frequency persists. As a result, a small peak of

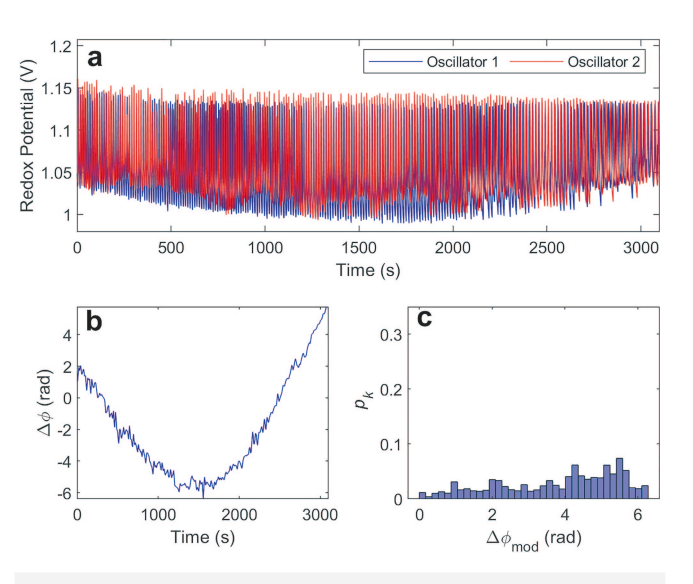


**FIG. 6.** Two electrochemically isolated BZ oscillators in the H-cell with high acid concentration ([ $H_2SO_4$ ] = 1.4M). (a) Evolution of redox potential vs time. (b) Phase difference vs time. (c) Probability distribution of  $\Delta\phi_{mod}$ .

0.07 is seen in Fig. 6(c) at 5.5 rad. The entropy remains high at 3.42, which is 96% of  $S_{max}$ .

When the oscillators are coupled under high concentration of acid, synchronization is observed in Fig. 7(a). The synchronization can be confirmed by the phase difference shown in Fig. 7(b). The phase difference remains relatively constant throughout the entire time series. As a result, a peak of 0.14 is seen at 5.1 rad in Fig. 7(c),

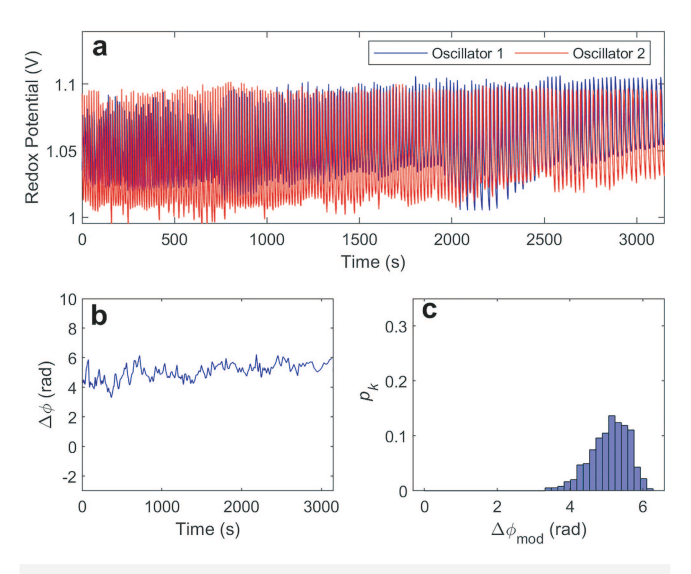


**FIG. 7.** Two electrochemically coupled BZ oscillators in the H-cell with high acid concentration ([H<sub>2</sub>SO<sub>4</sub>] = 1.4M). (a) Evolution of redox potential vs time. (b) Phase difference vs time. (c) Probability distribution of  $\Delta\phi_{mod}$ .

and the entropy decreases to 2.48, which is 69% of  $S_{max}$ . In this case,  $\Delta\phi_{mod}$  distributed only between  $\pi$  and  $2\pi$  rad, and  $p_k$  in the other half is 0. This indicates strong coupling strength between the two oscillators. The increased coupling strength can be interpreted by the decreased solution (electrolyte) and charge transfer resistance due to the increased H<sup>+</sup> concentration.

# B. Model and simulation

### 1. Oregonator model

A detailed, now widely accepted mechanism of the BZ reaction was proposed by Field, Körös, and Noyes (FKN).<sup>8</sup> The mechanism can be reduced to a three-variable model, the "Oregonator,"<sup>9,54</sup> which still predicts the salient dynamical features of the system. The Oregonator is commonly written in five irreversible steps, whose rate constants are related to proton concentrations. The reaction scheme is as follows:

$$A + Y \longrightarrow X + P$$
, Rate =  $k_1[A][Y]$ ,  $k_1 = k_{R3}[H^+]^2$ , (3)

$$X + Y \longrightarrow P + P$$
, Rate =  $k_2[X][Y]$ ,  $k_2 = k_{R2}[H^+]$ , (4)

$$A + X \longrightarrow 2X + Z$$
, Rate =  $k_3[A][X]$ ,  $k_3 = k_{R5}[H^+]$ , (5)

$$X + X \longrightarrow A + P$$
, Rate =  $k_4[X]^2$ ,  $k_4 = k_{R4}[H^+]$ , (6)

$$B + Z \longrightarrow fY$$
, Rate =  $k_5[B][Z]$ , (7)

with the following identities: X=[HBrO<sub>2</sub>], Y=[Br-], Z=[Ce(IV)], A = [BrO<sub>3</sub>-], B = [CH<sub>2</sub>(COOH)<sub>2</sub>], P = [HOBr], and f is a stoichiometric adjustable factor. The rate constants for the reactions are labeled  $k_1$  to  $k_5$ , which are related to the rate constants ( $k_{R2}$  to  $k_{R5}$ ) in the original FKN mechanism and the concentration of the acid. The values used here are as follows:  $k_1 = 2 \, \text{M}^{-3} \, \text{s}^{-1}$ ,  $k_2 = 1 \times 10^6 \, \text{M}^{-2} \, \text{s}^{-1}$ ,  $k_3 = 10 \, \text{M}^{-2} \, \text{s}^{-1}$ , and  $k_4 = 2000 \, \text{M}^{-1} \, \text{s}^{-1}$  for [H+] = 1.5 M.<sup>55</sup>

The three-variable dimensionless equations are scaled and reduced based on the FKN mechanism

$$\varepsilon \frac{dx}{d\tau} = qay - xy + ax - x^2,\tag{8}$$

$$\gamma \frac{dy}{d\tau} = -qay - xy + fbz, \tag{9}$$

$$\frac{dz}{d\tau} = ax - bz. ag{10}$$

The progression of time  $\tau$  in the simulations is reported in arbitrary units (a.u.). The dynamic variables x, y, and z represent the concentrations of HBrO<sub>2</sub>, Br—, and Ce(IV), respectively.

In the Oregonator model, the principal oscillatory variables are X ([HBrO<sub>2</sub>]), Y ([Br-]), and Z ([Ce(IV)]), while A ([BrO<sub>3</sub>-]) and B ([CH<sub>2</sub>(COOH)<sub>2</sub>]) are considered at much higher concentrations and remain constant. In our experiments under batch condition, however, the concentrations of A and B decrease over time. In

order to simulate our experimental conditions, two additional variables are added into the original dimensionless equations (8)–(10) according to the kinetics in the model,

$$\alpha \frac{da}{d\tau} = -qay - ax + x^2,\tag{11}$$

$$\beta \frac{db}{d\tau} = -bz,\tag{12}$$

where  $\alpha = 270$  and  $\beta = 430$  are time-scale parameters. ( $\alpha >> 1$  and  $\beta >> 1$  choices ensure that the species A and B are slowly decaying rather than quickly varying.) The terms in Eqs. (11) and (12) were derived from mass action kinetics of the mechanism in Eqs. (3)–(7).

For two oscillators, an additional set of equations was added,

$$\varepsilon \frac{dx'}{d\tau} = qa'y' - x'y' + a'x' - x'^2, \tag{13}$$

$$\gamma \frac{dy'}{d\tau} = -qa'y' - x'y' + fb'z',\tag{14}$$

$$\frac{dz'}{d\tau} = a'x' - b'z',\tag{15}$$

$$\alpha \frac{da'}{d\tau} = -qa'y' - a'x' + x'^2, \tag{16}$$

$$\beta' \frac{db'}{d\tau} = -b'z',\tag{17}$$

where  $\beta' = 412.8$ , and the 'indicates variables and parameter of the second oscillator. (This  $\beta' = 412.8$  choice reflects the slightly different kinetic conditions in the second reactor, e.g., due to mixing, geometry, temperature fluctuations, or surface conditions.)

When the two oscillators are connected through the metal wire and the Pt mesh, the different oxidation status in the two reactors builds up a potential difference. We assume this potential difference is mainly contributed to the metal catalyst, whose concentration is several orders of magnitude higher than any other oscillatory species. The coupling term we used in the simulation is similar to the one used by Crowley and Field<sup>44</sup> and is based on the Nernst equation. Current flows between the two oscillators as a result of the potential difference between the metal catalyst. The magnitude of the current will depend on the conductivity and acidity of the solution. In the presence of coupling, Eqs. (10) and (15) now become

$$\frac{dz}{d\tau} = ax - bz + k \ln \frac{(1-z)z'}{z(1-z')},$$
(18)

$$\frac{dz'}{d\tau} = a'x' - b'z' - k \ln \frac{(1-z)z'}{z(1-z')}.$$
 (19)

The coupling strength (*k*) is a complicated function of hydrogen concentration, and it depends nonlinearly on the conductivity, electrochemical reaction rate, mass/charge transfer coefficient, and geometry of the cell. To represent this nonlinear feature

in a simplified phenomenological approach, we took a quadratic dependence,

$$k = \kappa [H]^2, \tag{20}$$

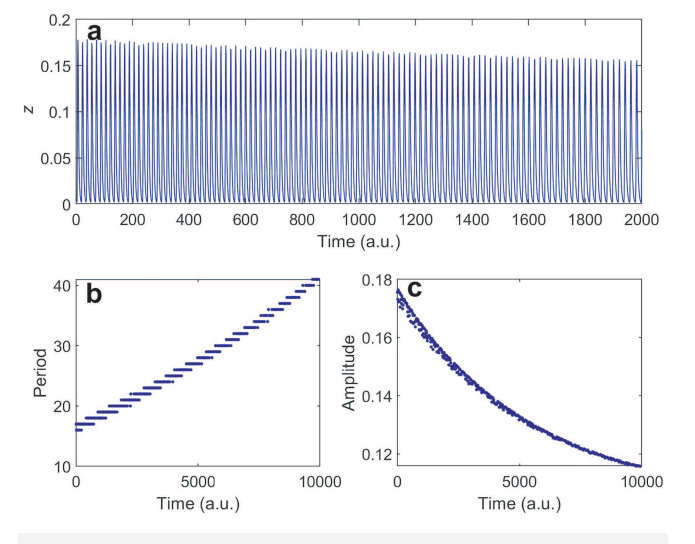
where  $\kappa=1.1\times 10^{-5}$  is the conductivity and H is the hydrogen ion concentration of the solution. In high acid concentration, H=3; otherwise, H=1.5.

# 2. Simulation of a single oscillator

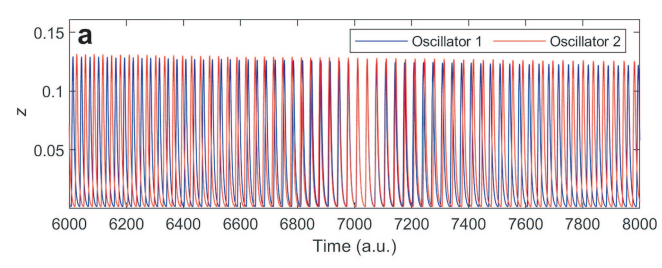
Numerical simulations of a single oscillator were performed with Eqs. (8)–(12). Figure 8(a) shows the oscillation of variable z, which is the metal catalyst, for the first 109 cycles. Similar to the experiments in Fig. 2, the distance between the peak of each cycle becomes slightly larger and the amplitude of the oscillations gradually decreases. These can be confirmed in Figs. 8(b) and 8(c), where the period increases from 16 to 41, and the amplitude decreases from 0.176 to 0.116. With good agreement between the experiment and simulation for a single oscillator, we then move on to two oscillators.

# 3. Simulation of two uncoupled oscillators for low acid concentration

Equations (8)–(17) were used for two uncoupled oscillators. Figure 9(a) shows that the oscillations nearly overlap at t=7000 a.u. and drift away before and after. The phase difference in Fig. 9(b) decreases at the beginning and reaches its minimum at t=2200 a.u., and then it starts to increase until the end of the times series. This is similar to the experiment in Fig. 3(b). Moreover, the  $\Delta \phi_{mod}$  distribution in Fig. 9(c) shows a small peak of 0.08 similar to Fig. 3(c) close to  $\pi$ . The entropy is 3.43, which is 96% of  $S_{max}$ , similar to that in the experiment (97%).



**FIG. 8.** Simulation of a single BZ oscillator with low acid concentration (H=1.5). (a) Evolution of z vs time. (b) Instantaneous period vs time. (c) Instantaneous amplitude vs time. Other parameters are the same in all simulations:  $\varepsilon=0.0667, \gamma=8.89\times10^{-5}, q=8\times10^{-4}, \alpha=270,$  and  $\beta=430.$ 



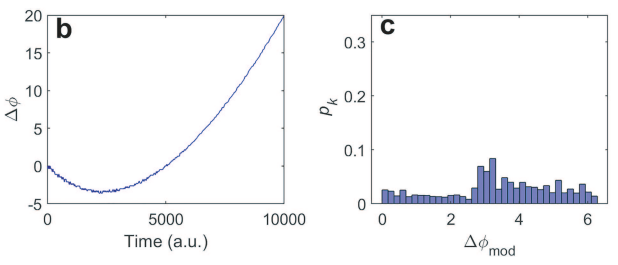


**FIG. 9.** Simulation of two uncoupled BZ oscillators with low acid concentration (H=1.5). (a) Concentration z vs time. (b) Phase difference vs time. (c) Probability distribution of  $\Delta\phi_{mod}$ .  $\beta'=412.8$ . In-phase, identical initial conditions were used with  $x_0=0$ ,  $y_0=3.287$ ,  $z_0=0.006225$ ,  $z_0=0.4$ , and  $z_0=0.4$  for both oscillators

In the following simulation, we changed the initial conditions and the probability distributions of  $\Delta\phi_{mod}$  are shown in Fig. 10. With out-of-phase initial condition [Fig. 10(a)], the highest peak is 0.08 at 5 rad, and two slightly smaller peaks are observed to the left with height of 0.06 and 0.07. With anti-phase initial conditions [Fig. 10(b)], the peak value is 0.09 at 1.5 rad. Comparison of Figs. 9(c), 10(a), and 10(b) reveals that changing the initial conditions changes the peak position but not the peak height. Thus, the simulations confirm the experiments that peaks in the phase difference histogram can be obtained even with uncoupled oscillators, but such small peaks, whose position varies with initial conditions, do not reflect the presence of coupling.

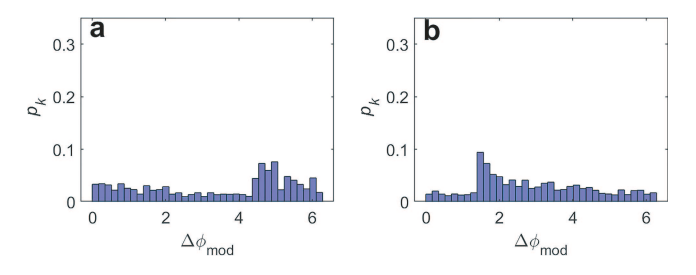


**FIG. 10.** Probability distribution of  $\Delta\phi_{mod}$  in simulation (H=1.5) showing different peak positions. (a) Initial condition: Out-of-phase. (For oscillator 2:  $x_0'=0$ ,  $y_0'=24.26$ ,  $z_0'=0.045$  15,  $a_0'=0.4$ , and  $b_0'=0.404$ .) (b) Initial condition: Anti-phase. (For oscillator 2:  $x_0'=0.1411$ ,  $y_0'=0$ ,  $z_0'=0.061$  09,  $a_0'=0.4$ , and  $a_0'=0.4$ ). For oscillator 1, the initial condition is the same as in Fig. 9.

# 4. Simulation of two coupled oscillators for low acid concentration

When coupling is introduced to the system, Eqs. (10) and (15) in the set [Eqs. (8)-(17)] are replaced by Eqs. (18) and (19). The coupling strength is defined by Eq. (20), and in this case, k = 2.475 $\times$  10<sup>-5</sup>. Figure 11(a) demonstrates an anti-phase region of oscillation, when one oscillator reaches the peak and the other is at the trough. In Fig. 11(b), the phase difference shows some small plateaus similar to the experiment [Fig. 5(b)] at 6564 and 7460 a.u. in the time series. Furthermore, from 2000 to 6000 a.u., there is a relatively flat region where the phase difference increases very slowly from  $-\pi$  to  $-\frac{\pi}{2}$ . This slow change causes the distribution of  $\Delta\phi_{mod}$ in Fig. 11(c) to show a very low value between 0 and  $\pi$ , and a peak value of 0.12 is observed at  $\pi$ . In the region between  $\pi$  and  $2\pi$ ,  $p_k$ decreases gradually, which corresponds to the slow change in phase difference from 2000 to 6000 a.u. in Fig. 11(b). These result in a slight decrease in entropy to 3.13, which is now 87% of  $S_{max}$ . We noticed that in Fig. 9(c), without coupling, a peak is seen around  $\pi$  as well. The introduction of the coupling strength increases the peak height while it is not strong enough to maintain the phase difference at  $\pi$ . The coupling strength is weak under low acid concentration, and we increased the concentration of proton in the simulation to further explore the coupling effect.

# 5. Simulation of two coupled oscillators for high acid concentration

When the proton concentration is increased to H=3, the effective coupling strength is increased by four times, and  $k=9.9 \times 10^{-5}$ . An inspection of the time series in Fig. 12(a) reveals out-of-phase synchronization: the peaks follow each other with a small time-lag. This can be further proved by the phase difference for the

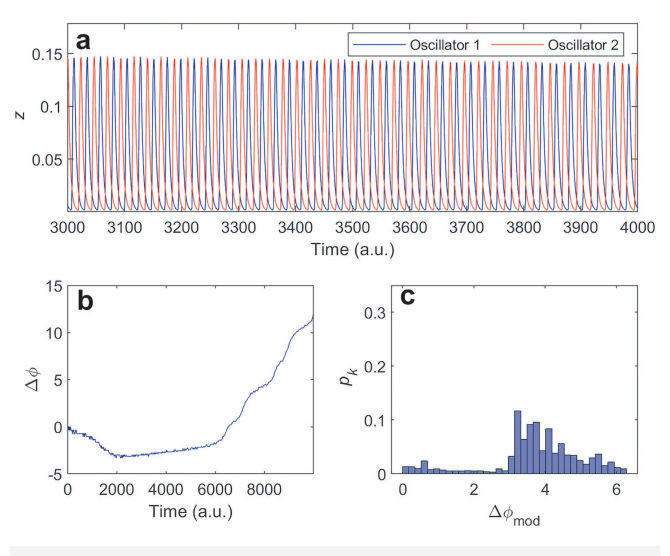


**FIG. 11.** Simulation of two electrochemically coupled BZ oscillators with low acid concentration (H=1.5). (a) Concentration z vs time. (b) Phase difference vs time. (c) Probability distribution of  $\Delta\phi_{mod}$ .  $k=2.475\times10^{-5}$ .

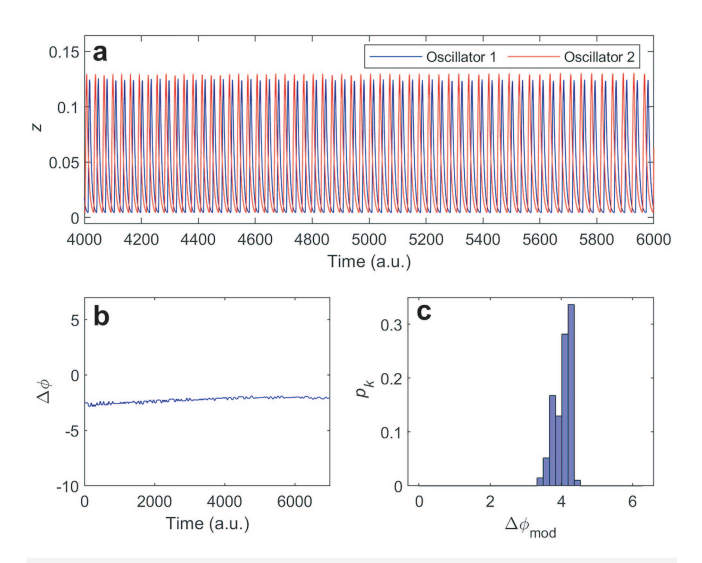


**FIG. 12.** Simulation of two electrochemically coupled BZ oscillators with high acid concentration (H=3). (a) Concentration z vs time. (b) Phase difference vs time. (c) Probability distribution of  $\Delta\phi_{mod}$ .  $k=9.9\times10^{-5}$ .

entire time series (0–7000 a.u.) in Fig. 12(b).  $\Delta \phi_{mod}$  in Fig. 12(c) is distributed mainly around 4 rad and is zero outside the narrow region. A high peak of 0.34 around 4.3 rad is observed. These lead to a large *decrease* in entropy to 1.56 (44% of  $S_{max}$ ). The simulations, thus, confirm that at an increased acid concentration the passive coupling can synchronize the oscillations.

#### IV. CONCLUSIONS

We showed that BZ oscillators can be coupled through the potential difference between  $Ru(byp)_3^{2+}/Ru(byp)_3^{3+}$  redox couple without external feedback. Under batch conditions, due to the consumption of bromate and malonic acid, the system is characterized by a large drift in the natural frequencies of oscillators, which slow down over time. With low acid concentration, electrochemically coupled oscillators showed a nonlinear phase difference with an extremum. However, the coupling was very weak and this feature was not mainly due to coupling, as we have also seen such curve in uncoupled oscillators. Based on the initial frequencies of the two oscillators can occur. At the time close to the intersection, the frequencies of the two oscillators become very close. The extremum of the phase difference reflects where the frequencies intersect.

In such systems, an effective way to characterize the coupling effect is to use the Gibbs–Shannon entropy of the cyclic phase difference. With low acid concentration, the probability distribution of  $\Delta\phi_{mod}$  showed a peak and the entropy decreased compared to the uncoupled cases, but the decrease was slight at around 10% of the maximum entropy. The coupling strength can be increased with higher concentration of sulfuric acid while the concentrations of other reactants remain the same. In this case, in spite of the large drift in the system, synchronization between the two oscillators was

observed. The entropy in this case *decreased* by 30% when out-of-phase synchronization was observed. In many cases, inspection of the phase difference time series provides a straightforward way to show the coupling-induced synchronization. In highly drifting chemical systems, the entropy provides a quantitative measure of the coupling strength, whereas the phase difference hardly distinguishes the absence of coupling from weakly coupled cases. Thus, we presented a systematic way to analyze the coupling effect in a highly drifting nonlinear system. Such highly drifting systems are expected to occur in biological rhythms, for example, where it was shown that the circadian rhythm of golden hamster and deermouse had progressively shorter periods as the animals became older.<sup>56</sup>

The observed synchronization behavior in experiments using BZ oscillators were reproduced in numerical simulations based on the Oregonator model. Two additional variables were introduced with adjusted parameters in order to account for the drifting behavior. The model successfully captured all the main features of single, uncoupled, and coupled oscillators. Transition to synchronization can be achieved by an enhanced coupling introduced to account and adjust the proton concentration as in the experiments.

These results, thus, show that electrochemical coupling can provide sufficient ion exchange for synchronization between chemical oscillators in a spontaneous process. This coupling resembles the communication among neurons where both short-distance chemical signals and long-distance electrical signals are sent. Such coupling can open avenues for design of rich synchronization patterns, <sup>57</sup> e.g., clustering and chimeras, similar to those achieved with actively coupled BZ beads<sup>18</sup> or electrochemical oscillators. <sup>58</sup> Finally, our results can also be of interest when combined with chemical computing automata, such as chemical Turing machines, <sup>59,60</sup> in their application to neuromorphic chemical computation.

# **ACKNOWLEDGMENTS**

We would like to thank Dick Field for his pioneering work that inspired many of the phenomena we investigated throughout our careers and, in particular, sparked our interest in the topic of this manuscript on electrochemically coupled BZ oscillators. I.Z.K. acknowledges support from the National Science Foundation (NSF) under Grant No. CHE-1900011. J.P.-M. thanks Repsol, S.A. for their funding of this work and their continued support. Y.L. was supported by both the NSF and Repsol through the above grants. The funders had no role in study design, data collection and analysis, decision to publish, or preparation of the manuscript.

# **AUTHOR DECLARATIONS**

# Conflict of Interest

The authors have no conflicts to disclose.

#### **Author Contributions**

Yifan Liu: Conceptualization (equal); Investigation (equal); Writing – original draft (lead); Writing – review & editing (equal). Juan Pérez-Mercader: Conceptualization (equal); Investigation (equal); Writing – review & editing (equal). István Z. Kiss:

Conceptualization (equal); Investigation (equal); Writing – review & editing (equal).

#### **DATA AVAILABILITY**

The data that support the findings of this study are available from the corresponding author upon reasonable request.

### **REFERENCES**

- <sup>1</sup>I. R. Epstein, "Coupled chemical oscillators and emergent system properties," Chem. Commun. **50**, 10758–10767 (2014).
- <sup>2</sup>A. F. Taylor, M. R. Tinsley, and K. Showalter, "Insights into collective cell behaviour from populations of coupled chemical oscillators," Phys. Chem. Chem. Phys. 17, 20047–20055 (2015).
- <sup>3</sup>I. R. Epstein and K. Showalter, "Nonlinear chemical dynamics: Oscillations, patterns, and chaos," J. Phys. Chem. 100, 13132–13147 (1996).
- <sup>4</sup>Y. Kuramoto, Chemical Oscillations, Waves & Turbulence (Springer, Berlin, 1984)
- <sup>5</sup>M. A. Budroni, G. Pagano, D. Conte, B. Paternoster, R. D'ambrosio, S. Ristori, A. Abou-Hassan, and F. Rossi, "Synchronization scenarios induced by delayed communication in arrays of diffusively coupled autonomous chemical oscillators," Phys. Chem. Chem. Phys. 23, 17606–17615 (2021).
- <sup>6</sup>G. Philippou and D. Luss, "Temperature patterns on a catalytic ribbon heated by a constant voltage," Chem. Eng. Sci. **48**, 2313–2323 (1993).
- <sup>7</sup>I. Z. Kiss, Y. Zhai, and J. L. Hudson, "Emerging coherence in a population of chemical oscillators," Science 296, 1676–1678 (2002).
- <sup>8</sup>R. J. Field, E. Koros, and R. M. Noyes, "Oscillations in chemical systems. II. Thorough analysis of temporal oscillation in the bromate-cerium-malonic acid system," J. Am. Chem. Soc. **94**, 8649–8664 (1972).
- <sup>9</sup>R. J. Field and R. M. Noyes, "Oscillations in chemical systems. IV. Limit cycle behavior in a model of a real chemical reaction," J. Chem. Phys. **60**, 1877–1884 (1974).
- <sup>10</sup>Oscillations and Traveling Waves in Chemical Systems, edited by R. J. Field and M. Burger (Wiley, New York, 1985).
- <sup>11</sup>M. Marek and I. Stuchl, "Synchronization in two interacting oscillatory systems," Biophys. Chem. 3, 241–248 (1975).
- <sup>12</sup>I. Stuchl and M. Marek, "Dissipative structures in coupled cells: Experiments," J. Chem. Phys. 77, 2956–2963 (1982).
- <sup>13</sup>M. F. Crowley and I. R. Epstein, "Experimental and theoretical studies of a coupled chemical oscillator: Phase death, multistability and in-phase and out-of-phase entrainment," J. Phys. Chem. 93, 2496–2502 (1989).
  <sup>14</sup>H. Fujii and Y. Sawada, "Phase-difference locking of coupled oscillating chemi-
- <sup>14</sup>H. Fujii and Y. Sawada, "Phase-difference locking of coupled oscillating chemical systems," J. Chem. Phys. 69, 3830–3832 (1978).
- <sup>15</sup>A. F. Taylor, M. R. Tinsley, F. Wang, Z. Huang, and K. Showalter, "Dynamical quorum sensing and synchronization in large populations of chemical oscillators," Science **323**, 614–617 (2009).
- <sup>16</sup>M. R. Tinsley, S. Nkomo, and K. Showalter, "Chimera and phase-cluster states in populations of coupled chemical oscillators," Nat. Phys. 8, 662–665 (2012).
- <sup>17</sup>A. F. Taylor, M. R. Tinsley, F. Wang, and K. Showalter, "Phase clusters in large populations of chemical oscillators," Angew. Chem. Int. Ed. **50**, 10161–10164 (2011).
- <sup>18</sup>J. F. Totz, J. Rode, M. R. Tinsley, K. Showalter, and H. Engel, "Spiral wave chimera states in large populations of coupled chemical oscillators," Nat. Phys. 14, 282–285 (2018).
- <sup>19</sup>N. Tompkins, N. Li, C. Girabawe, M. Heymann, G. Ermentrout, I. R. Epstein, and S. Fraden, "Testing Turing's theory of morphogenesis in chemical cells," Proc. Natl. Acad. Sci. U.S.A. 111, 4397–4402 (2014).
- <sup>20</sup> M. M. Norton, N. Tompkins, B. Blanc, M. C. Cambria, J. Held, and S. Fraden, "Dynamics of reaction-diffusion oscillators in star and other networks with cyclic symmetries exhibiting multiple clusters," Phys. Rev. Lett. 123, 148301 (2019).
- <sup>21</sup> M. Wickramasinghe and I. Z. Kiss, "Synchronization of electrochemical oscillators," in *Engineering of Chemical Complexity* (World Scientific, New Jersey, 2013), pp. 215–236.

- <sup>22</sup>D. K. Verma, H. Singh, A. Q. Contractor, and P. Parmananda, "Synchronization in autonomous mercury beating heart systems," J. Phys. Chem. A 118, 4647–4651 (2014).
- (2014). <sup>23</sup>T. Singla, F. Montoya, M. Rivera, S. Tajima, S. Nakabayashi, and P. Parmananda, "Synchronization using environmental coupling in mercury beating heart oscillators," Chaos **26**, 063103 (2016).
- <sup>24</sup>P. Kumar, D. K. Verma, P. Parmananda, and S. Boccaletti, "Experimental evidence of explosive synchronization in mercury beating-heart oscillators," Phys. Rev. E 91, 062909 (2015).
- <sup>25</sup> A. Biswas, D. Das, and P. Parmananda, "Scaling dependence and synchronization of forced mercury beating heart systems," Phys. Rev. E **95**, 042202 (2017).
- (2017). <sup>26</sup> A. Biswas, P. Kumar, D. Das, and P. Parmananda, "Oscillatory activity regulation in an ensemble of autonomous mercury beating heart oscillators," Phys. Rev. E **99**, 032223 (2019).
- <sup>27</sup>P. Kumar and P. Parmananda, "Control, synchronization, and enhanced reliability of aperiodic oscillations in the mercury beating heart system," Chaos 28, 045105 (2018).
- <sup>28</sup>S. Tajima, H. Singh, S. Nakabayashi, T. Singla, and P. Parmananda, "The emergence of synchrony behavior in weakly coupled electrochemical oscillators via a 'metallic plate," J. Electroanal. Chem. **769**, 16–20 (2016).
- <sup>29</sup>B. K. Bera, D. Ghosh, P. Parmananda, G. V. Osipov, and S. K. Dana, "Coexisting synchronous and asynchronous states in locally coupled array of oscillators by partial self-feedback control," Chaos 27, 073108 (2017).
  <sup>30</sup>F. Montoya, M. Rivera, J. Escalona, and P. Parmananda, "Construction of
- <sup>30</sup>F. Montoya, M. Rivera, J. Escalona, and P. Parmananda, "Construction of Arnold tongue structures for coupled periodic oscillators," Phys. Lett. A **377**, 3124–3127 (2013).
- <sup>31</sup>R. Nagao, W. Zou, J. Kurths, and I. Z. Kiss, "Restoring oscillatory behavior from amplitude death with anti-phase synchronization patterns in networks of electrochemical oscillations," Chaos **26**, 094808 (2016).
- $^{32}$ M. Wickramasinghe and I. Z. Kiss, "Spatially organized dynamical states in chemical oscillator networks: Synchronization, dynamical differentiation, and chimera patterns," PLoS One 8, e80586 (2013).
- <sup>33</sup>Y. Liu, M. Sebek, F. Mori, and I. Z. Kiss, "Synchronization of three electrochemical oscillators: From local to global coupling," Chaos **28**, 045104 (2018).
- <sup>34</sup> M. Wickramasinghe, E. M. Mrugacz, and I. Z. Kiss, "Dynamics of electrochemical oscillators with electrode size disparity: Asymmetrical coupling and anomalous phase synchronization," Phys. Chem. Chem. Phys. 13, 15483–15491 (2011).
  <sup>35</sup> I. Z. Kiss and J. L. Hudson, "Phase synchronization of nonidentical chaotic
- <sup>35</sup>I. Z. Kiss and J. L. Hudson, "Phase synchronization of nonidentical chaotic electrochemical oscillators," Phys. Chem. Chem. Phys. 4, 2638–2647 (2002).
- <sup>36</sup>I. Z. Kiss, W. Wang, and J. L. Hudson, "Complexity of globally coupled chaotic electrochemical oscillators," Phys. Chem. Chem. Phys. 2, 3847–3854 (2000).
- <sup>37</sup>I. Z. Kiss, Y. Zhai, and J. L. Hudson, "Predicting mutual entrainment of oscillators with experiment-based phase models," Phys. Rev. Lett. **94**, 248301 (2005).
- (2005). <sup>38</sup> M. J. Hankins, V. Gáspár, and I. Z. Kiss, "Abrupt and gradual onset of synchronized oscillations due to dynamical quorum sensing in the single-cathode multi-anode nickel electrodissolution system," Chaos **29**, 033114 (2019).
- <sup>39</sup> A. S. Mikhailov, D. H. Zanette, Y. M. Zhai, I. Z. Kiss, and J. L. Hudson, "Cooperative action of coherent groups in broadly heterogeneous populations of interacting chemical oscillators," Proc. Natl. Acad. Sci. U.S.A. 101, 10890–10894 (2004).
- <sup>40</sup>J. L. Ocampo-Espindola, C. Bick, and I. Z. Kiss, "Weak chimeras in modular electrochemical oscillator networks," Front. Appl. Math. Stat. 5, 38 (2019).

- <sup>41</sup> L. Schmidt, K. Schönleber, K. Krischer, and V. García-Morales, "Coexistence of synchrony and incoherence in oscillatory media under nonlinear global coupling," Chaos 24, 013102 (2014).
- <sup>42</sup>Y. Jia and I. Z. Kiss, "Spontaneously synchronized electrochemical micro-oscillators with nickel electrodissolution," J. Phys. Chem. C **116**, 19290–19299 (2012)
- (2012). <sup>43</sup>Y. Liu and I. Z. Kiss, "Localization of current oscillations and synchronization patterns in microchip-based dual electrode flow cell without resistance balancing," Eur. Phys. J. Spec. Top. **227**, 2659–2673 (2019).
- <sup>44</sup>M. F. Crowley and R. J. Field, "Electrically coupled Belousov-Zhabotinsky oscillators: A potential chaos generator," in *Nonlinear Phenomena in Chemical Dynamics*, edited by C. Vidal and A. Pacault (Springer, Berlin, 1981), pp. 147–153.
   <sup>45</sup>M. F. Crowley and R. J. Field, "Electrically coupled Belousov-Zhabotinskii oscillators: Experimental observation of chaos in a chemical system and identification of its source in the Field-Noyes equations," in *Nonlinear Oscillations in Biology and Chemistry*, edited by H. G. Othmer (Springer, Berlin, 1986), pp. 68–97.
- <sup>46</sup> M. F. Crowley and R. J. Field, "Electrically coupled Belousov-Zhabotinskii oscillators. 1. Experiments and simulations," J. Phys. Chem. 90, 1907-1915 (1986).
- <sup>47</sup>W. Hohmann, N. Schinor, M. Kraus, and F. W. Schneider, "Electrically coupled chemical oscillators and their action potentials," J. Phys. Chem. A **103**, 5742–5748 (1999).
- (1999). <sup>48</sup> A. Guderian, A. F. Münster, M. Kraus, and F. W. Schneider, "Electrochemical chaos control in a chemical reaction: Experiment and simulation," J. Phys. Chem. A **102**, 5059–5064 (1998).
- <sup>49</sup>G. Dechert, K.-P. Zeyer, D. Lebender, and F. W. Schneider, "Recognition of phase patterns in a chemical reactor network," J. Phys. Chem. **100**, 19043–19048 (1996).
- <sup>50</sup>W. Hohmann, M. Kraus, and F. W. Schneider, "Recognition in excitable chemical reactor networks. Experiments and model-simulations," J. Phys. Chem. A **101**, 7364–7370 (1997).
- <sup>51</sup>W. Hohmann, M. Kraus, and F. W. Schneider, "Learning and recognition in excitable chemical reactor networks," J. Phys. Chem. A 102, 3103–3111 (1998).
- <sup>52</sup>W. Hohmann, M. Kraus, and F. W. Schneider, "Pattern recognition by electrical coupling of eight chemical reactors." J. Phys. Chem. A **103**, 7606–7611 (1999)
- coupling of eight chemical reactors," J. Phys. Chem. A 103, 7606–7611 (1999). <sup>53</sup> A. Adamatzky, B. De Lacy Costello, and T. Asai, *Reaction-Diffusion Computers* (Elsevier Science, 2005).
- 54]. J. Tyson, "Scaling and reducing the Field-Koros-Noyes mechanism of the Belousov-Zhabotinskii reaction," J. Phys. Chem. 86, 3006–3012 (1982).
- <sup>55</sup>K. Sriram, "Effects of positive electrical feedback in the oscillating Belousov–Zhabotinsky reaction: Experiments and simulations," Chaos Solitons Fractals 28, 1055–1066 (2006).
- <sup>56</sup>C. S. Pittendrigh and S. Daan, "Circadian oscillations in rodents: A systematic increase of their frequency with age," Science 186, 548–550 (1974).
- <sup>57</sup>I. Z. Kiss, "Synchronization engineering," Curr. Opin. Chem. Eng. 21, 1–9 (2018).
- <sup>58</sup> M. Sebek and I. Z. Kiss, "Spatiotemporal patterns on a ring network of oscillatory electrochemical reaction with negative global feedback," Isr. J. Chem. **58**, 753–761 (2018).
- <sup>59</sup>M. Dueñas-Díez and J. Pérez-Mercader, "How chemistry computes: Language recognition by non-biochemical chemical automata. From finite automata to turing machines," iScience 19, 514–526 (2019).
- <sup>60</sup>M. Dueñas-Díez and J. Pérez-Mercader, "Native chemical computation. A generic application of oscillating chemistry illustrated with the Belousov-Zhabotinsky reaction. A review," Front. Chem. 9, 204 (2021).